Fuel 140 (2015) 803–809

Contents lists available at ScienceDirect

Fuel

journal homepage: www.elsevier.com/locate/fuel

The cooperation of Fe—Sn in a MnO_x complex sorbent used for capturing elemental mercury

Haomiao Xu, Jiangkun Xie, Yongpeng Ma, Zan Qu *, Songjian Zhao, Wanmiao Chen, Wenjun Huang, Naiqiang Yan *

School of Environmental Science and Engineering, Shanghai Jiao Tong University, Shanghai 200240, China

HIGHLIGHTS

- The Fe—Sn—Mn sorbent exhibited better performance on Hg^0 removal than pure MnO_x.
- The Fe—Sn—Mn sorbent had a wide temperature window when used.
- Fe and Sn were helpful for enlarging the BET surface areas of pure MnO_x.
- Fe could protect manganese active sites from SO_2 poison.

GRAPHICAL ABSTRACT

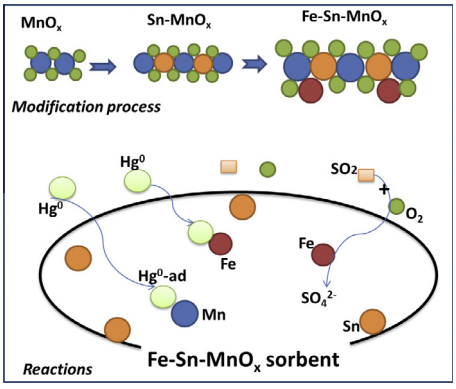

ARTICLE INFO

Article history:
Received 23 April 2014
Received in revised form 14 August 2014
Accepted 1 October 2014
Available online 18 October 2014

Keywords:
Manganese
Elemental mercury (Hg^0)
Fe—Sn modification
Sorbent

ABSTRACT

Manganese oxide (MnO_x) was an effective sorbent for capturing elemental mercury (Hg^0) from coal-fired flue gas, but its usage was markedly limited by its lower porosity, lower temperature range, and sensitivity to sulfur dioxide (SO_2). Tin (Sn) and iron (Fe) were tested for their ability to enhance MnO_x sorbent, and the Fe—Sn—MnO_x complex exhibited excellent performance as a novel mercury sorbent. SnO_2 appeared to be inert for Hg^0 adsorption, but it could act as a suitable support to disperse MnO_x, which helps to produce more activated sites. The BET surface areas increased by approximately 10 times, and there was an increase of 3 times the Hg^0 adsorption capacity. The available temperature range of the sorbent can be extended from 100 to 300 °C. Specifically, the presence of Fe can significantly improve the SO_2 resistance of the sorbent. Furthermore, the mechanism of adsorption and SO_2 tolerance at high temperatures was investigated by in situ Diffuse Reflectance Infrared Fourier Transform spectra (DRIFTs); Fe reacted with SO_2 when O_2 was present, which could protect manganese active sites from being poisoned by SO_2.

1. Introduction

The Minamata Convention on Mercury was adopted in October of 2013, and it is an international treaty aimed at protecting human health and the environment from anthropogenic mercury emissions. Mercury has long been known to be toxic to humans and other organisms. The famous Minamata disease was a large-scale public health crisis because of its toxic effects [1]. According to data calculated by Pirrone et al., approximately 2320 tons of mercury is emitted by human activities annually. Approximately 35% of the emissions result from fossil fuel combustion [2]. China

* Corresponding authors. Tel./fax: +86 21 54745591.
E-mail addresses: quzan@sjtu.edu.cn (Z. Qu), nqyan@sjtu.edu.cn (N. Yan).

http://dx.doi.org/10.1016/j.fuel.2014.10.004
0016-2361/

is by far the largest consumer of coal in the world, and approximately 70% of China's electrical generation comes from coal-fired power plants. Chinese anthropogenic sources account for more than 25% of total global mercury emissions according to Feng et al. [3]. Researchers have estimated that mercury emissions from anthropogenic sources will increase in several years [4–6]. Therefore, preventing the release of mercury from coal-fired power plants will continue to be a challenge.

Mercury is released into exhaust gas as elemental mercury (Hg^0), oxidized mercury (Hg^{2+}) and particulate bound mercury (Hg^p). At present, Hg^{2+} and Hg^p can generally be effectively removed by air pollution control devices (APCDs) [7–9]. However, Hg^0 is the most difficult to capture because of its high volatility and low solubility in water. This type of mercury can circulate in the atmosphere for years, and its toxic effects have a global-scale impact [10]. Many efforts had been made to remove Hg^0 from flue gas; there are two major methods for Hg^0 capture [11–13] as follows: (1) Oxidation, which transforms Hg^0 to Hg^{2+}. (2) Adsorption, transforms Hg^0 to Hg^p. Through the oxidation method, soluble Hg^{2+} matters were carried into desulfurizing solution or desulfurization gypsum along with flue gas. A large gypsum product (8.5×10^6 t a^{-1}) was derived from wet flue gas desulfurization (WFGD) systems. However, approximately 55% of the mercury was lost during manufacturing processes, which led to mercury secondary contamination in the atmosphere [14–16]. Hg^p can be collected through the adsorption method by fabric filter (FF) or electrostatic precipitator (ESP). This mercury can be enriched by high temperature separation or magnetic separation technology. Thus, the adsorption method seems to be an effective and green technology.

Activated carbon injection (ACI) technology is a simple and effective method for Hg^0 capture. Unfortunately, this technology has been not widely used in Chinese coal-fired power plants because of its high cost [7,17–20]. Furthermore, the low chlorine concentration in coal limits the technology for being widely used, and the chlorine concentration has been suggested as a factor that clearly affects Hg^0 removal efficiency from flue gas. Numerous studies have been performed to find an economic and efficacious sorbent as an alternative. Chemically modified active carbon, fly ash, Ca-based sorbents and metal oxide sorbents were often used in labs or in full scale research [19,21–24]. Because of its high removal efficiency and stability, metal oxide has attracted attention from investigators. Manganese oxide (MnO_x) sorbent seems to be a very good candidate. This compound has been used for removing Hg^0 from flue gas and as a selective catalytic reduction (SCR) catalyst in the past [25]. Yan et al. reported that an MnO_x support on inert alumina (α-Al_2O_3) could be used for Hg^0 removal at lower temperatures (100–200 °C). However, the effects of sulfur dioxide (SO_2) on Hg^0 adsorption were remarkable [26]. Several metal elements were employed as dopants to modify the MnO_x sorbent and facilitate the removal efficiency of Hg^0. Wiatros-Motyka et al. reported that the MnO_x/ZrO_2 sorbent adsorbs twice as much Hg^0 as activated carbon, and the rate of Hg^0 capture on the particle surface areas depends on the manganese content [27]. High surface area ceria-titania materials were used as supports for MnO_x for warm-gas Hg^0 capture (175 °C), which also exhibited an excellent mercury capture capacity [28]. Experiments by Yang et al. showed that Mn—Fe_2O_3 exhibited an excellent Hg^0 removal capacity, and it had better performance for SO_2 resistance than MnO_x [29]. Fe might be helpful for minimizing the infiltration of SO_2 to the sorbent. However, the application of MnO_x was still markedly limited by this material's lower porosity, lower temperature range, and its sensitivity to SO_2.

Tin dioxide (SnO_2) is usually regarded as an oxygen-deficient n-type semiconductor [30]. Our recent preliminary work indicated that Sn—Mn binary metal oxides could increase the BET surface areas. It can also be used within a broad temperature window (100–300 °C). However, SnO_2 had low SO_2 resistance at high temperatures. The addition of Fe was used to enhance the SO_2 resistance at high temperatures. With inspiration from these results and discussion, the objective of the present study is to investigate the cooperation of Sn and-Fe modified MnO_x for Hg^0 adsorption.

Herein, a series of Sn and Fe-doped MnO_x sorbents were prepared for Hg^0 removal within a high temperature window (100–300 °C), and the SO_2 impacts were also investigated in this study. The roles of Sn, Fe and MnO_x and the influence of SO_2 were discussed, taking into account the results of BET, XRD, TEM and in situ Diffuse Reflectance Infrared Fourier Transform spectra (DRIFTs).

2. Experimental

2.1. Sorbent Preparation

The sorbents were prepared using a co-precipitation method. Suitable amounts of $Fe(NO_3)_3$, $SnCl_4$ and $Mn(NO_3)_2$ were dissolved in distilled water. A stoichiometric amount of ammonia was added to the mixture as the precipitation agent under strong stirring for 2 h. For Fe—Sn—MnO_x (Fe:Sn:Mn = 1:20:20), 20 mmol $SnCl_4$, 20 mmol $Mn(NO_3)_2$ and 1 mmol $Fe(NO_3)_3$ were dissolved in 100 ml of deionized water under stirring. Afterwards, 123 mmol of ammonia was added to the mixed solution under strong stirring for 2 h. The precipitate was then filtered and washed with deionized water three times to remove Cl^- from the water. Lastly, the precipitate was transferred to a muffle furnace and calcined at 500 °C for 5 h. All of the samples were ground to a 40–60 mesh size.

2.2. Sorbent characterization

Measurements of the BET surface areas were performed on a Quantachrome Nova 2200e Automated Gas Sorption system. All samples were degassed at 200 °C in a nitrogen flow prior to N_2 physisorption at −196 °C. The crystal structure was determined using powder X-ray Diffraction Patterns (XRD) (APLX-DUO, BRUKER, Germany), and the scanning range was from 10° to 80° with a scanning velocity of 7° min^{-1} with Cu K radiation. The microstructure of the sorbent was analyzed by transmission electronic microscopy (TEM). The TEM image was created on a JEOLJEM-2010 TEM. The micrographs were obtained in bright-field imaging mode at an acceleration voltage of 200 kV. In situ DRIFT spectra were recorded on a Fourier transform infrared spectrometer (FTIR, Nicolet 6700) equipped with a smart collector and an MCT detector cooled by liquid N_2. Mass flow controllers and a sample temperature controller were used to simulate the real reaction conditions. Prior to each experiment, the sorbent was heated to the target temperature in N_2. And the component of flue gas (O_2, SO_2) was introduced in the simulate gas. The IR spectra were recorded by accumulating 100 scans at a resolution of 4 cm^{-1}. H_2-TPR experiment was performed on Chemisorp TPx 2920 instrument, the sorbents were degased at 300 °C for 3 h under Ar atmosphere before H_2-TPR test, the reducing gas was 10%H_2/Ar. Ion chromatography (EP-100) was used to detect SO_4^{2-} in the leachate, which was collected by washing the sorbent in ultrapure water after adsorption.

2.3. Elemental mercury capture

The process flow of the Hg^0 capacity assessment system is depicted in Fig. A1. The experimental facility consisted of an Hg^0 permeation tube, a fixed-bed reactor with a parallel blank tube, a cold vapor atomic absorption spectrometer (CVAAS) and an online data acquisition system. The Hg^0 removal capacity of the sorbents (40–60 mesh) was measured in the fixed-bed quartz reactor under the following reaction conditions: 30 mg sorbent, 4% O_2, and 1.25

(±0.05) mg/m^3 of Hg^0, all of which was balanced in N_2 with a total gas flow rate of 200 ml/min. To test the impact of the temperature on the Hg^0 adsorption performance, the experiments were performed within a temperature range from 100 to 300 °C. To test the influence of SO_2, 500–1000 ppm of SO_2 were introduced into the gaseous influent through a mass flow controller, and the total flow rate was also balanced with N_2. The Hg^0 concentrations of gaseous influent and effluent were continuously measured by a CVAAS (SG 921, Jiang fen Ltd., China), which was calibrated by a Lumex RA 915 + mercury analyzer.

To investigate the effects of the temperature and SO_2 concentration in the flue gas, the breakthrough curve areas for Hg^0 on Fe—Sn—MnO_x sorbents during the test time (10 h or 20 h) was integrated and the adsorption capacities of Hg^0 were calculated according to Eq. (1).

$$Q = \frac{1}{m}\int_{t2}^{t1}\left(Hg^0_{in} - Hg^0_{out}\right) \times f \times dt \quad (1)$$

where Q is the Hg^0 adsorption capacity, m is the mass of the sorbent in the fixed-bed, f denotes the flow rate of the influent, and t_0 and t_1 represent the initial and ending test time of the breakthrough curves.

3. Results and discussion

3.1. Elemental mercury capture performance

In this work, prepared pure metal oxides and complex metal oxide sorbents for Hg^0 adsorption were tested using a fixed-bed experimental facility. Fig. 1 shows the Hg^0 adsorption capacity at different temperatures. Pure SnO_2 sorbent showed nearly no activity for Hg^0 capture at 100–300 °C. Pure FeO_x also exhibited a low capacity. By contrast, pure MnO_x had a higher adsorption capacity, and the Hg^0 capacity could reach approximately 2 mg/g at 100 °C. However, this capacity clearly decreased with the increasing temperature, and the capacity at 300 °C was only a quarter of the capacity at 100 °C.

To improve the Hg^0 capture performance of the MnO_x sorbent, Fe and Sn were used for modification on the MnO_x sorbent. The performances of Fe—MnO_x, Fe—SnO_2, Sn—MnO_x and Fe—Sn—MnO_x complex metal oxide sorbents are shown in Fig. 1. The molar ratio of Fe:Sn:Mn was 1:20:20 in each sorbent. With the Fe—MnO_x sorbent, the doped Fe can increase the adsorption capacity, with an increase by approximately 50% at 100 °C. However, the Hg^0 adsorption capacity of Fe—MnO_x still markedly decreased with the temperature increase. In addition, the Fe—SnO_2 metal oxide sorbent displayed far less Hg^0 capture capacity in comparison with Fe—MnO_x, but its capacity increased slightly as the temperature went up. The Sn—MnO_x sorbent had a higher Hg^0 capacity compared with Fe—SnO_2 and Fe—MnO_x sorbents, and it could reach approximately 3 mg/g at 100 °C. Moreover, the adsorption capacity of Hg^0 also increased slightly as the temperature rose. The Sn—MnO_x sorbent displayed a wide temperature window for Hg^0 adsorption. Additionally, the Fe doped to Sn—MnO_x further enhanced the Hg^0 adsorption capacity, and the Hg^0 adsorption capacity for Fe—Sn—MnO_x increased by approximately 20–30% in comparison with Sn—MnO_x. Fe—Sn—MnO_x also had a wide temperature window for Hg^0 adsorption. Obviously, Sn played an important role in enhancing the high temperature activity. H_2-TPR technology was employed to collect the reducing information during the temperature-programmed process. The results were shown in Fig. A2. Sn—Mn binary metal oxides appeared at 200–600 °C and the peaks turned to high temperature along with the increasing of Sn. The reducing peak of SnO_2 emerged at higher than 600 °C. It could indicate that adding Sn into MnO_x expands the temperature window of MnO_x sorbent.

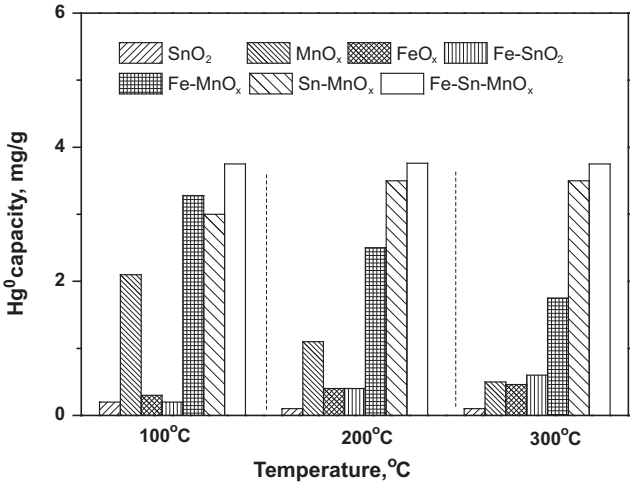

Fig. 1. Temperature impact on the Hg^0 adsorption capacity (10 h) of the prepared sorbents.

Sorbents with different Fe contents were prepared and evaluated to investigate the Fe effect in Fe—Sn—MnO_x. As shown in Fig. 2, the Hg^0 adsorption capacity (20 h) slightly decreases with the increased Fe concentration. An Fe molar percentage of 2–5% in the sorbent appeared to be enough for the modification (the molar ratio of Fe:Sn:Mn was 1:20:20 in the following section). Therefore, Mn was the primary active site for Hg^0 adsorption, Fe also had a capacity for Hg^0 to some extent, and Sn could improve the high temperature activity for Hg^0 capture.

3.2. The physiochemical characterization of Fe and Sn modified MnO_x

BET, XRD and TEM were employed for structural analysis to reveal the cooperative effects of Sn and Fe on MnO_x. Table 1 summarizes the BET surface areas. The results show that the BET

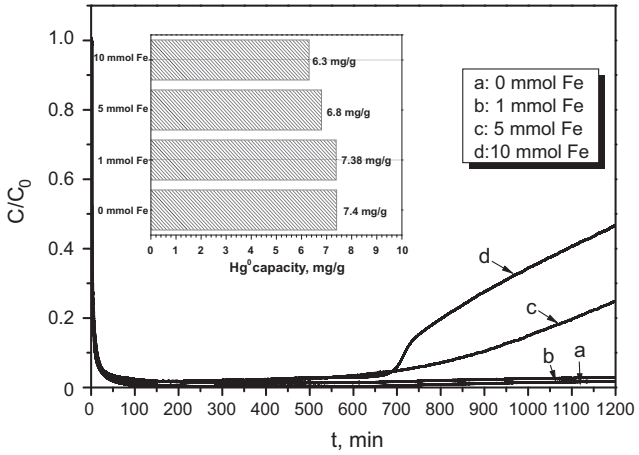

Fig. 2. The impact of different Fe concentrations on the Fe—Sn—MnO_x sorbent for Hg^0 removal.

Table 1
BET surface areas of prepared sorbents.

Sorbents	BET surface areas (m^2/g)
SnO_2	25.5
MnO_x	5.3
FeO_x	18.7
Sn—MnO_x	53.9
Fe—SnO_2	64.3
Fe—MnO_x	21.9
Fe—Sn—MnO_x	74.5

surface areas of pure SnO_2, MnO_x and FeO_x were 25.2, 5.3 and 18.7 m^2/g, respectively. With the addition of Sn to the MnO_x, the BET surface areas of Sn—MnO_x were approximately two times larger than pure MnO_x, and they expanded to 53.9 m^2/g. Upon adding approximately 2.5% Fe to Sn—MnO_x, Fe—Sn—MnO_x exhibited the largest BET surface areas among the prepared sorbents, reaching up to 74.5 m^2/g. Such large surface areas could provide more active sites on MnO_x sorbents, which was beneficial for the adsorption. The BET surface areas of Fe—SnO_2 also reached as high as 64.3 m^2/g. This finding indicated that the existence state of SnO_2 was greatly changed by adding Fe. However, the BET surface areas of the Fe—MnO_x sorbents were only 21.9 m^2/g. Therefore, SnO_2 appeared to be an excellent support for dispersing Fe or Mn atoms, which would dramatically increase the BET surface areas for the sorbents.

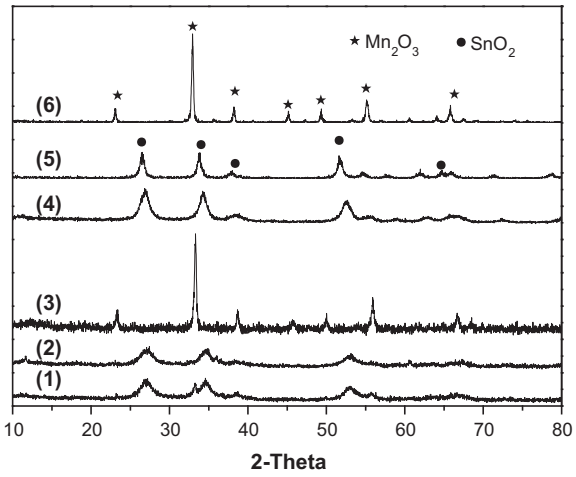

Fig. 3. The XRD patterns of the prepared sorbents. (1) Fe—Sn—MnO_x; (2) Sn—MnO_x; (3) Fe—MnO_x; (4) Fe—SnO_2; (5) SnO_2; and (6) MnO_x.

Fig. 3 illustrates the XRD patterns of Fe—Sn—MnO_x, Sn—MnO_x, Fe—MnO_x, Fe—SnO_2, pure SnO_2 and pure MnO_x metal oxides. The peaks at 23°, 33°, 38°, 50°, 56° and 67° for pure MnO_x were attributed to the Mn_2O_3 structure (PDF#31-0825).The XRD pattern of Fe—MnO_x had almost the same peaks. Fe—Sn—MnO_x, Sn—MnO_x, and Fe—SnO_2 all had the same peak at $2\theta = 27°$, 34°, 53°, and 67°, respectively. The same peaks were also found in pure SnO_2 patterns. This finding could definitely be attributed to the same crystal structure of SnO_2 (PDF#41-1445). Therefore, most of the Mn atoms were doped into the crystal lattice of SnO_2 and changed the lattice parameter, and employing such a small amount of Fe did not clearly affect the crystal structure of complex oxides [31]. Furthermore, the diffraction peaks of Fe—Sn—MnO_x, Sn—MnO_x and Fe—SnO_2 became broader in comparison with pure SnO_2 peaks, so smaller particle sizes tended to form. The results were consistent with the BET data.

TEM was also employed to further study the morphology of the prepared sorbents. As shown in Fig. 4, the Fe—MnO_x particles were much larger than the other sorbents. The size of the Fe—SnO_2, Sn—MnO_x and Fe—Sn—MnO_x particles were all approximately 10–20 nm. In comparison with Sn—MnO_x particles, evenly spherical particles could be observed for Fe—Sn—MnO_x. This shape can provide more chances to form Mn active sites on these particles. Thus, in synthesizing the above results, SnO_2 could serve as an

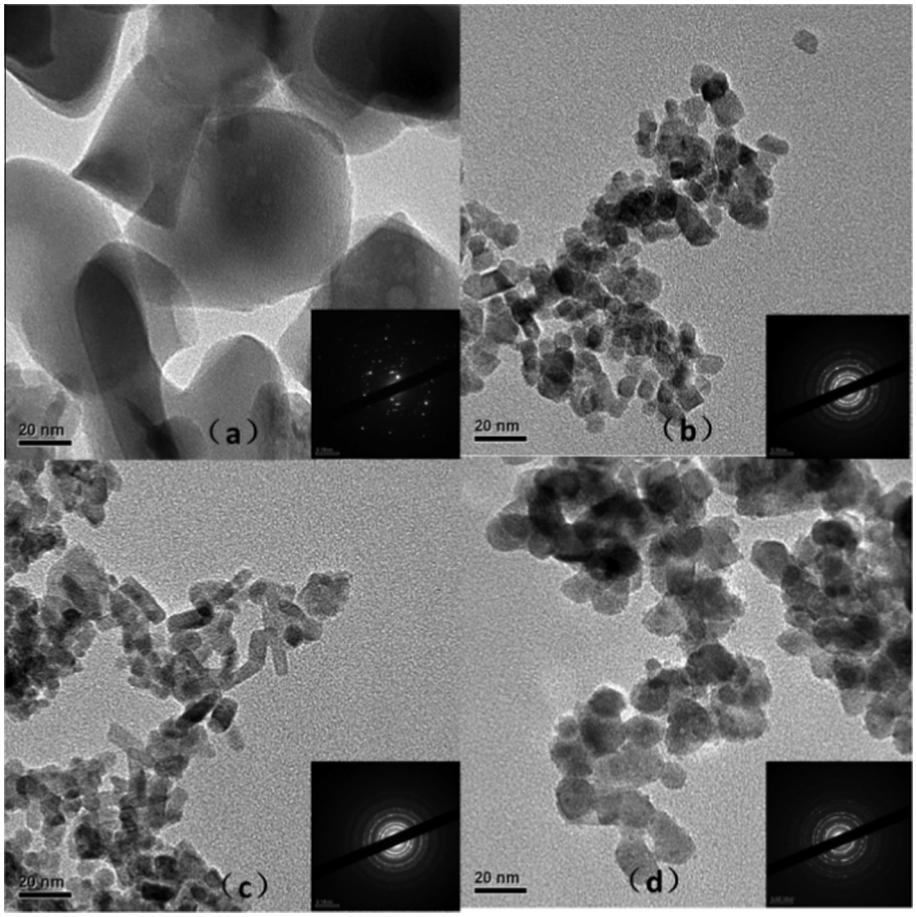

Fig. 4. TEM images of the prepared sorbents. (a) Fe—MnO_x; (b) Fe—SnO_2; (c) Sn—MnO_x; and (d) Fe—Sn—MnO_x.

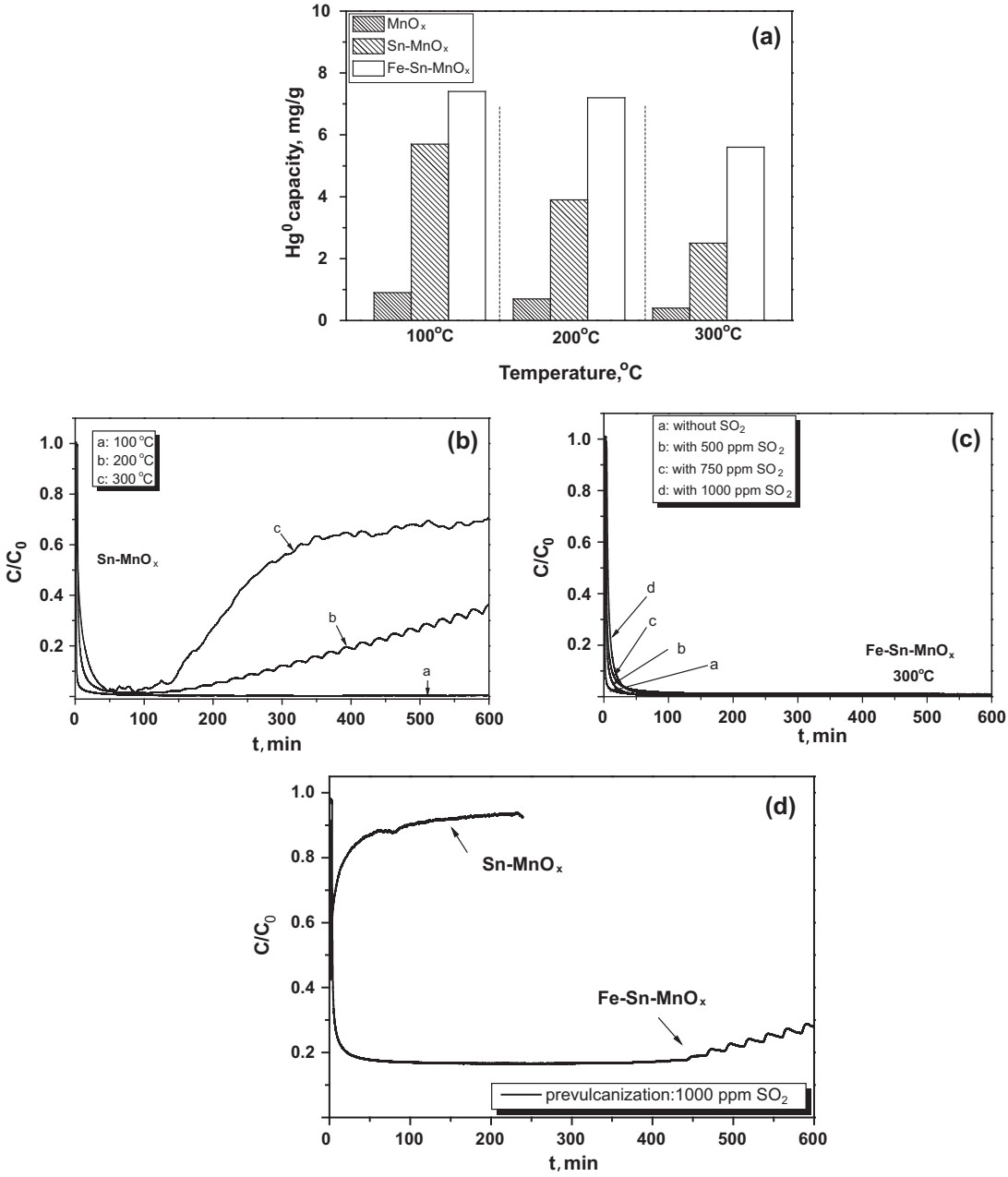

Fig. 5. The impact of SO_2 on the Hg^0 adsorption of the sorbents. (a) Hg^0 capacity in 20 h; (b) Sn—MnO_x, SO_2 concentration: 500 ppm; (c) Fe—Sn—MnO_x, temperature: 300 °C; and (d) pre-vulcanization with 1000 ppm SO_2 (10 h).

excellent support to disperse Mn. Mn atoms could enter into the crystal lattice of SnO_2 [32]. The presence of Fe in the sorbent can improve the dispersion of Mn in the sorbent. With the addition of the Sn and Fe atoms, the BET surface areas of MnO_x increased sharply. These characteristics of the prepared sorbent will provide the potential ability for Hg^0 adsorption on the sorbent surface.

3.3. SO_2 effects

3.3.1. Hg^0 capture performance

In general, the SO_2 concentration is hundreds of times higher than that of Hg^0 [33]. Therefore, the effect of SO_2 on Hg^0 adsorption should be taken into account. Fig. 5(a) shows the Hg^0 adsorption capacity for 20 h of pure MnO_x, Sn—MnO_x and Fe—Sn—MnO_x sorbents. Notably, the pure MnO_x and Sn—MnO_x sorbent capacity for Hg^0 decreased along with the temperature increase when SO_2 was present. These compounds had a weak SO_2 tolerance at high temperatures. Therefore, the Mn active component may not have higher temperature-tolerant activity in the presence of SO_2 [34]. The higher temperature could degrade this component's performance in Hg^0 capture when SO_2 is present. SO_2 may compete with gaseous Hg^0 for the activity sites. Thus, the sorbents were poisoned by SO_2 during the adsorption process, which could be explained by the follow reaction [35]:

$$SO_2(g) + \equiv Mn^{4+} + \equiv O_2 \rightarrow \equiv Mn^{4+} - SO_4 \quad (2)$$

According to the above reaction, the Mn active sites were occupied by sulfate. For the Fe—Sn—MnO_x sorbent, there was a better performance at 300 °C than that of pure MnO_x and Sn—MnO_x when SO_2 was present. The Hg^0 capacity could reach 2 times greater than that of Sn—MnO_x. Fig. 5(b) indicated that the Hg^0 capacity of Sn—MnO_x decreased with the temperature increase when SO_2

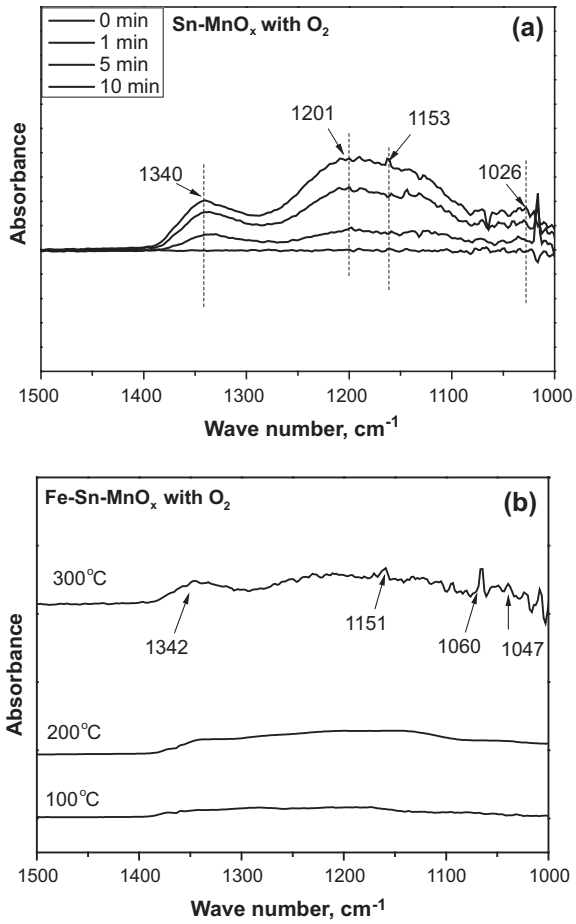

Fig. 6. (a) DRIFT spectra taken at 300 °C upon passing O_2 over Sn—MnO_x; (b) DRIFT spectra taken at 100–300 °C upon passing O_2 over Fe—Sn—MnO_x (10 min).

was present. The results in Fig. 5(c) exhibited excellent SO_2 tolerance at various SO_2 concentrations of Fe—Sn—MnO_x sorbent at 300 °C. The Fe in the Fe—Sn—MnO_x sorbent was excellent at resisting SO_2 at high temperatures. To verify this phenomenon, an additional experiment was performed by pre-vulcanizing the sorbents in the gas with 1000 ppm SO_2 for 10 h, and the results are shown in Fig. 5(d). Sn—MnO_x lost nearly all its capacity for Hg^0 capture, but the Fe—Sn—MnO_x sorbent remained at more than 80% of the Hg^0 capture efficiency within 10 h at 300 °C. Apparently, Fe plays an important role in SO_2 tolerance, and its mechanism will be discussed in the following section.

3.3.2. DRIFTs study for the mechanism of SO_2 on the surface of the sorbents

As mentioned above, both Sn—MnO_x and Fe—Sn—MnO_x sorbents exhibited good performance in terms of the Hg^0 capacity within a wide temperature window. However, Sn/MnO_x seems to be impacted by SO_2 at high temperatures. SO_2 showed comparatively less inhabitation to Fe—Sn—MnO_x for Hg^0 adsorption at different temperature ranges. DRIFTs were employed to collect in-situ spectra data for investigating the mechanism of SO_2 impact at high temperatures in these two sorbents. As shown in Fig. 6(a), several peaks at 1340, 1201, 1153 and 1026 cm^{-1} emerged, and the intensity increased with the exposure time. The peak at 1340 cm^{-1} could be attributed to the ν(S=O) vibration of the surface sulfate species with only one S=O band [36]. Peaks at 1201, 1153 and 1026 cm^{-1} could be assigned to the stretching motion of adsorbed bisulfate or sulfate on the surface of the sorbent [36]. Moreover, the higher the temperature was, the more sulfate species could be found. It was speculated that SO_2 reacts with manganese at high temperatures, and the sulfate species formed on the surface of the sorbent, which would inhibit the Hg^0 adsorptive property. In Fig. 6(b), only small peaks could be found in the spectra when 4% O_2 was added to the simulated flue gas. These broad absorbance bands between 1000 and 1300 cm^{-1} were assigned to the stretching mode of adsorbed bisulfate, HSO_4^-, and/or sulfate, SO_4^{2-}, on the surface of the sorbent [37]. Ion chromatography was used to determine the sulfate formed on the surface of the sorbent. The sulfate was detected and the results are shown in Fig. A3. Therefore, the mechanism for Fe—Sn—MnO_x tolerance of SO_2 may be that Fe can preferentially react with SO_2 when O_2 was present, which can prevent MnO_x from combining with SO_2.

3.4. The Hg^0 capture mechanism on Fe—Sn—MnO_x sorbents

In combining the results and characterization, the mechanism of Hg^0 adsorbed on the surface can be illustrated as follows. MnO_x was the primary active component for Hg^0 capture. Fe oxide also had Hg^0 capacity to some extent [29]. The binary Sn—Mn metal oxide sorbent had a higher adsorption capacity compared with the MnO_x sorbent, and it can be used within a wide temperature window. The resulting Fe—Sn—MnO_x complex sorbent had the highest capacity among the sorbents, which could also be used within a wide temperature interval. The role of Sn and Fe clearly improved the performance of MnO_x. The Hg^0 captured by metal oxide sorbents may be attributed to the Mars–Maessen mechanism [8,11,19]. The possible reactions for Hg^0 on the surface of the Fe—Sn—Mn—O_x sorbent are as follows:

$$Hg(g) \rightarrow \equiv Hg(ads) \quad (3)$$

$$\equiv Hg(ads) + \equiv Fe{-}Sn{-}MnO_x \rightarrow \equiv HgO(ads) + \equiv Fe{-}Sn{-}MnO_{x-1} \quad (4)$$

$$\equiv Fe{-}Sn{-}MnO_{x-1} + 1/2O_2 \rightarrow \equiv Fe{-}Sn{-}MnO_x \quad (5)$$

$$\equiv HgO(ads) + \equiv Fe{-}Sn{-}MnO_x \rightarrow \equiv Fe{-}Sn{-}MnO_{x+1} \quad (6)$$

Sn enlarged the BET surface areas of MnO_x when Mn entered the lattice of the SnO_2 metal oxide. Fe further influenced the enlarging surface areas of Sn—Mn binary metal oxides. SnO_2 provided excellent support for Mn and Fe in the Fe—Sn—MnO_x complex sorbent according to the physiochemical characterization results. Sn plays another role in enhancing the activity at high temperatures for MnO_x. The doped Fe could further enhance the dispersibility of Mn in the Fe—Sn—Mn complex oxides. Fe also exhibits excellent performance at high temperatures. The doped Fe solved another problem in that the Sn—Mn binary lost its Hg^0 capacity to some extent when SO_2 was present at high temperatures. The synthesized Fe—Sn—MnO_x had excellent performance in terms of Hg^0 capture and SO_2 tolerance within a wide temperature window.

4. Conclusions

Fe—Sn—Mn complex oxide sorbents were synthesized and evaluated for their effective removal of Hg^0 from simulated flue gas. BET results showed that Fe—Sn—MnO_x had the largest BET surface areas among the prepared sorbents. The adsorption capacity of Hg^0 could reach as high as 3.75 mg/g in 10 h. It can also be used within a wide temperature range with SO_2. The physiochemical characterization shows that Sn and Fe play important roles in enlarging the BET surface areas, which provide the possibility for more Mn active sites. Moreover, Fe could protect the Mn active sites at high temperatures from SO_2 poisoning.

Acknowledgments

This study was supported by the Major State Basic Research Development Program of China (973 Program, No. 2013CB430005),

the National Natural Science Foundation of China (No. 50908145, No. 21277088) and the National High-Tech R&D Program (863) of China (No. 2011AA060801, No. 2013AA065403). Ms. Xiaofang Hu is acknowledged for the assistance in DRIFT analysis.

Appendix A. Supplementary material

The Hg^0 capacity assessment system, H_2-TPR and ion chromatography are in the Appendices. Supplementary data associated with this article can be found, in the online version, at http://dx.doi.org/10.1016/j.fuel.2014.10.004.

References

[1] Harada M. Minamata disease: methylmercury poisoning in Japan caused by environmental pollution. CRC Crit Rev Toxicol 1995;25:1–24.
[2] Pirrone N, Cinnirella S, Feng X, Finkelman R, Friedli H, Leaner J, et al. Global mercury emissions to the atmosphere from anthropogenic and natural sources. Atmos Chem Phys 2010;10:5951–64.
[3] Fu X, Feng X, Sommar J, Wang S. A review of studies on atmospheric mercury in China. Sci Total Environ 2012;421:73–81.
[4] Streets DG, Zhang Q, Wu Y. Projections of global mercury emissions in 2050. Environ Sci Technol 2009;43:2983–8.
[5] Pacyna EG, Pacyna J, Sundseth K, Munthe J, Kindbom K, Wilson S, et al. Global emission of mercury to the atmosphere from anthropogenic sources in 2005 and projections to 2020. Atmos Environ 2010;44:2487–99.
[6] Lin C-J, Gustin MS, Singhasuk P, Eckley C, Miller M. Empirical models for estimating mercury flux from soils. Environ Sci Technol 2010;44:8522–8.
[7] Gao Y, Zhang Z, Wu J, Duan L, Umar A, Sun L, et al. A critical review on the heterogeneous catalytic oxidation of elemental mercury in flue gases. Environ Sci Technol 2013;47:10813–23.
[8] Pavlish JH, Sondreal EA, Mann MD, Olson ES, Galbreath KC, Laudal DL, et al. Status review of mercury control options for coal-fired power plants. Fuel Process Technol 2003;82:89–165.
[9] Lin C-J, Pongprueksa P, Lindberg SE, Pehkonen SO, Byun D, Jang C. Scientific uncertainties in atmospheric mercury models I: model science evaluation. Atmos Environ 2006;40:2911–28.
[10] Driscoll CT, Mason RP, Chan HM, Jacob DJ, Pirrone N. Mercury as a global pollutant: sources, pathways, and effects. Environ Sci Technol 2013;47:4967–83.
[11] Presto AA, Granite EJ. Survey of catalysts for oxidation of mercury in flue gas. Environ Sci Technol 2006;40:5601–9.
[12] Wilcox J, Rupp E, Ying SC, Lim D-H, Negreira AS, Kirchofer A, et al. Mercury adsorption and oxidation in coal combustion and gasification processes. Int J Coal Geol 2012;90:4–20.
[13] Yang H, Xu Z, Fan M, Bland AE, Judkins RR. Adsorbents for capturing mercury in coal-fired boiler flue gas. J Hazard Mater 2007;146:1–11.
[14] Truman C, Nuti R, Truman L, Dean J. Feasibility of using FGD gypsum to conserve water and reduce erosion from an agricultural soil in Georgia. Catena 2010;81:234–9.
[15] Liu X, Wang S, Zhang L, Wu Y, Duan L, Hao J. Speciation of mercury in FGD gypsum and mercury emission during the wallboard production in China. Fuel 2013;111:621–7.
[16] Tang T, Xu J, Lu R, Wo J, Xu X. Enhanced Hg^{2+} removal and Hg^0 re-emission control from wet fuel gas desulfurization liquors with additives. Fuel 2010;89:3613–7.
[17] Presto AA, Granite EJ. Impact of sulfur oxides on mercury capture by activated carbon. Environ Sci Technol 2007;41:6579–84.
[18] Galbreath KC, Zygarlicke CJ. Mercury transformations in coal combustion flue gas. Fuel Process Technol 2000;65:289–310.
[19] Granite EJ, Pennline HW, Hargis RA. Novel sorbents for mercury removal from flue gas. Ind Eng Chem Res 2000;39:1020–9.
[20] Zeng H, Jin F, Guo J. Removal of elemental mercury from coal combustion flue gas by chloride-impregnated activated carbon. Fuel 2004;83:143–6.
[21] Granite EJ, Pennline HW. Photochemical removal of mercury from flue gas. Ind Eng Chem Res 2002;41:5470–6.
[22] Dunham GE, DeWall RA, Senior CL. Fixed-bed studies of the interactions between mercury and coal combustion fly ash. Fuel Process Technol 2003;82:197–213.
[23] Li Y, Murphy P, Wu C-Y. Removal of elemental mercury from simulated coal-combustion flue gas using a SiO_2–TiO_2 nanocomposite. Fuel Process Technol 2008;89:567–73.
[24] Mei Z, Shen Z, Zhao Q, Wang W, Zhang Y. Removal and recovery of gas-phase element mercury by metal oxide-loaded activated carbon. J Hazard Mater 2008;152:721–9.
[25] Wu Z, Jin R, Liu Y, Wang H. Ceria modified MnO_x/TiO_2 as a superior catalyst for NO reduction with NH_3 at low-temperature. Catal Commun 2008;9:2217–20.
[26] Chang H, Chen X, Li J, Ma L, Wang C, Liu C, et al. Improvement of activity and SO_2 tolerance of Sn-modified MnO_x–CeO_2 catalysts for NH_3-SCR at low temperatures. Environ Sci Technol 2013;47:5294–301.
[27] Lin Q, Li J, Ma L, Hao J. Selective catalytic reduction of NO with NH_3 over Mn–Fe/USY under lean burn conditions. Catal Today 2010;151:251–6.
[28] He J, Reddy GK, Thiel SW, Smirniotis PG, Pinto NG. Ceria-modified manganese oxide/titania materials for removal of elemental and oxidized mercury from flue gas. J Phys Chem C 2011;115:24300–9.
[29] Yang S, Guo Y, Yan N, Wu D, He H, Xie J, et al. Remarkable effect of the incorporation of titanium on the catalytic activity and SO_2 poisoning resistance of magnetic Mn–Fe spinel for elemental mercury capture. Appl Catal B 2011;101:698–708.
[30] Joseph J, Mathew V, Abraham K. Studies on Cu, Fe, and Mn doped SnO_2 semiconducting transparent films prepared by a vapour deposition technique. Chin J Phys 2007;45:84–97.
[31] Tang X, Li J, Wei L, Hao J. MnO_x–SnO_2 catalysts synthesized by a redox coprecipitation method for selective catalytic reduction of NO by NH_3. Chin J Catal 2008;29:531–6.
[32] Xie J, Xu H, Qu Z, Huang W, Chen W, Ma Y, et al. Sn–Mn binary metal oxides as non-carbon sorbent for mercury removal in a wide-temperature window. J Colloid Interface Sci 2014;428:121–7.
[33] Chen J-C, Liu Z-S, Huang J-S. Emission characteristics of coal combustion in different O_2/N_2, O_2/O_2 and O_2/RFG atmosphere. J Hazard Mater 2007;142:266–71.
[34] Li J, Yan N, Qu Z, Qiao S, Yang S, Guo Y, et al. Catalytic oxidation of elemental mercury over the modified catalyst Mn/α-Al_2O_3 at lower temperatures. Environ Sci Technol 2009;44:426–31.
[35] Kijlstra WS, Biervliet M, PEELS E, Bliek A. Deactivation by SO_2 of MnO_x/Al_2O_3 catalysts used for the selective catalytic reduction of NO with NH_3 at low temperatures. Appl Catal B 1998;16:327–37.
[36] Jiang B, Wu Z, Liu Y, Lee S, Ho W. DRIFT study of the SO_2 effect on low-temperature SCR reaction over Fe–Mn/TiO_2. J Phys Chem C 2010;114:4961–5.
[37] Fu H, Xu T, Yang S, Zhang S, Chen J. Photoinduced formation of Fe (III)-sulfato complexes on the surface of r-Fe_2O_3 and their photochemical performance. J Phys Chem 2009;100:11316–22.